Impacts of Internally and Externally Mixed Anthropogenic Sulfate and Carbonaceous Aerosols on East Asian Climate*

ZHANG Li (张 力), LIU Hongnian†(刘红年), and ZHANG Ning (张 宁)

School of Atmospheric Sciences, Nanjing University, Nanjing 210093

(Received July 1, 2010; in final form March 22, 2011)

ABSTRACT

A coupled regional climate and aerosol-chemistry model, RIEMS 2.0 (Regional Integrated Environmental Model System for Asia), in which anthropogenic sulfate, black carbon, and organic carbon were assumed to be externally mixed (EM), internally mixed (IM) or partially internally mixed (IEM), was used to simulate the impacts of these anthropogenic aerosols on East Asian climate for the entire year of 2006. The distributions of aerosol mass concentration, radiative forcing and hence the surface air temperature and precipitation variations under three mixing assumptions of aerosols were analyzed. The results indicated that the mass concentration of sulfate was sensitive to mixing assumptions, but carbonaceous aerosols were much less sensitive to the mixing types. Modeled results were compared with observations in a variety of sites in East Asia. It was found that the simulated concentrations of sulfate and carbonaceous aerosols were in accord with the observations in terms of magnitude. The simulated aerosol concentrations in IM case were closest to observation results. The regional average column burdens of sulfate, black carbon, and organic carbon, if internally mixed, were 11.49, 0.47, and 2.17 mg m^{-2}, respectively. The radiative forcing of anthropogenic aerosols at the top of the atmosphere increased from –1.27 (EM) to –1.97 W m^{-2} (IM) while the normalized radiative forcing (NRF) decreased from –0.145 (EM) to –0.139 W mg^{-1} (IM). The radiative forcing and NRF were –1.82 W m^{-2} and –0.141 W mg^{-1} for IEM, respectively. The surface air temperature changes over the domain due to the anthropogenic sulfate and carbonaceous aerosols were –0.067, –0.078, and –0.072 K, with maxima of –0.47, –0.50, and –0.49 K, for EM, IM, and IEM, respectively. Meanwhile, the annual precipitation variations were –8.0 (EM), –20.6 (IM), and –21.9 mm (IEM), with maxima of 148, 122, and 102 mm, respectively, indicating that the climate effects were stronger if the sulfate and carbonaceous aerosols were internally mixed.

Key words: anthropogenic aerosols, externally mixed, internally mixed, climate effects

Citation: Zhang Li, Liu Hongnian, and Zhang Ning, 2011: Impacts of internally and externally mixed anthropogenic sulfate and carbonaceous aerosols on East Asian climate. *Acta Meteor. Sinica*, **25**(5), 639–658, doi: 10.1007/s13351-011-0508-7.

1. Introduction

Aerosols, from both anthropogenic and natural sources, affect the regional and global climate directly and indirectly. In highly industrial regions such as North America, Europe, and East Asia, the emissions of anthropogenic sulfate and carbonaceous aerosols are very large (IPCC, 2007). Anthropogenic sulfate and carbonaceous aerosols, including black carbon (BC) and organic carbon (OC), are two of the most important aerosols in these areas. Research focused on these two kinds of anthropogenic aerosols is becoming increasingly important. With rapid developments of economy and industrialization, the emissions of precursors of anthropogenic aerosols have continued to dramatically increase in East Asia since the 1980s, especially in China (Manktelow et al., 2007; Streets et al., 2008). Observations indicated that anthropogenic sulfate and carbonaceous aerosols were two major components of the aerosol mix in Asia in addition to dust (Bergin et al., 2001; Xu et al., 2002; Tan et al., 2004). Previous studies generally suggested that the surface air temperature and precipitation decreased in East Asia due to the anthropogenic aerosols when treated as an external mixture; and these reductions cannot be ignored (Giorgi et al., 2002, 2003;

*Supported by the National Key Basic Research and Development (973) Program of China (2006CB400506 and 2010CB428501) and National Natural Science Foundation of China (40775014).

†Corresponding author: liuhn@nju.edu.cn.

Qian et al., 2003; Gu et al., 2006; Huang et al., 2007; Han et al., 2008; Zhang et al., 2009a).

The diversity of aerosol types results in a complex mixture of aerosol components. Generally, the mixing state of aerosols can be divided into external mixing, internal mixing, and partial internal mixing. As an extreme, external mixing operates under the assumption that each aerosol component is physically separated from the other components. As the other extreme, internal mixing, aerosols are assumed to be internally mixed as a homogeneous material reflecting the chemical and physical average of all the contributing components. Between the external mixing state and internal mixing state, the partial internal mixing state mirrors the real mixing state in the atmosphere under the assumption that part of each aerosol component is internally mixed as a homogeneous mixture that simultaneously mixes with the remaining aerosols in an external mixing state.

An internal mixture of aerosols can be produced if more than one component is involved in the creation of aerosols. Even if the particles are individually pure when first produced, there are many processes in the atmosphere that can convert an external mixture to an internal mixture including coagulations, gas-to-particle reactions, and heterogeneous reactions onto existing particles. Some observations conducted in polluted cities of East Asia indicated that BC, OC, and sulfate could be strongly internally mixed (Moteki et al., 2007a, b; Shiraiwa et al., 2007, 2008), and similar phenomena were also observed in a clean city of East Asia (Li et al., 2010).

To date, for studies on aerosol effects on climate, most of the models have treated aerosols as an external mixture while a minority assumed internal mixing (Liao and Seinfeld, 2005) or partial internal mixing (Stier et al., 2005; Kim et al., 2008; Lu and Bowman, 2010).

The majority of earlier related studies, such as the studies of Glebard et al. (1980), Warren and Seinfeld (1985), and Kim and Seinfeld (1990), focused on the mixture of sulfate and BC, considered the two most important anthropogenic aerosol components. Fassi-Fihri et al. (1997) developed an internal and external model for sulfate and BC and compared the difference of optical properties and coagulations between the internal and external mixtures of these two aerosols. Recently, a detailed aerosol mixing state model was developed in Lu and Bowman (2010).

Research on externally and internally mixed aerosols can be extremely difficult due to the complexity and variability of the mixing state. The number fraction of the internal mixture varies from 0 to 80% with the size of the aerosol particles (Strom et al., 1992; Naoe and Okada, 2001), increases with the altitude (Schwarz et al., 2008), and evolves over time (Moteki et al., 2007b; Shiraiwa et al., 2007).

The morphology of the internal mixture is complex. The most common and elaborate morphology is a core-shell form in which insoluble BC acts as a core with soluble sulfate acting as shell (Ebert et al., 2002; Vester et al., 2007; Worringen et al., 2008).

The direct effects of anthropogenic aerosol on climate are primarily determined by the optical properties of the ensemble of aerosols, which in turn are determined by the size, morphology and chemical composition of the particles. The optical properties of internal mixtures are different from those of pure aerosol components (Lesins et al., 2002; Stier et al., 2006; Schwarz et al., 2008). BC can strongly absorb solar radiation and is estimated to be the second largest contributor to global warming after carbon dioxide (IPCC, 2007). While non-absorbing sulfate mainly scatters radiation and effectively increases albedo, it may also have acted to partly offset the effects of the absorption of BC as an external mixture. When sulfate and BC are internally mixed, the absorption of the mixture is greater than that of the pure sulfate component, and the ability of the internal mixture to scatter radiation is much greater than that of BC. The differences in optical properties between the external and internal mixtures of sulfate and BC have been discussed in several previous studies (Lesins et al., 2002; Stier et al., 2006; Schwarz et al., 2008; Shiraiwa et al., 2008). Lesins et al. (2002) found that the discrepancy of the extinction coefficient, single scattering albedo, and asymmetry factor between the external and internal mixtures reached as much as 25%–50%. Stier

et al. (2006) and Schwarz et al. (2008) found an increase in the absorption coefficient of BC when it was considered as internally mixed instead of externally mixed. Shiraiwa et al. (2008) also found that the absorption of the internal mixture containing BC was greater than that of the external mixture by a factor of 1.5 to 1.6 based on observations in East Asia. As the optical properties of an aerosol mixture change in different mixing states, the direct effect of multicomponent aerosols subsequently changes.

In addition to influencing the direct effect of aerosol, the mixing assumption influences the indirect effect by altering the deliquescence, water solubility, and size distribution of an aerosol mixture and, consequently, its efficiency of serving as cloud condensation nuclei (CCN), by which aerosols affect the radiative properties of clouds (Chung and Seinfeld, 2005).

To date, there has not been a comprehensive examination of the sensitivity of climate effects to the mixing assumptions made in a regional climate model for anthropogenic sulfate and carbonaceous carbon, including BC and OC. This paper focuses on the discrepancies of concentrations of anthropogenic sulfate, BC, and OC, and, hence, the radiative forcing and impacts on climate due to anthropogenic aerosols under the assumptions of an internal mixing state, external mixing state or partial internal mixing state. Section 2 contains brief descriptions of the model, experimental design, and data used in the model. The results are presented in Section 3, and the discussion and conclusions are found in Section 4.

2. Model description and experimental design

2.1 Model description

The regional climate model used in this study was the Regional Integrated Environmental Model System for Asia (RIEMS 2.0), developed by the START Regional Center for Temperate East Asia (START TEA RC) in Beijing, China (START: System for Analysis, Research, and Training) (Fu et al., 2000). RIEMS 2.0 is based on the third version of the fifth-generation Pennsylvania State University/National Center for Atmospheric Research mesoscale model (MM5v3) (Fu et al., 2000). The model processes include a state of the art surface physics package (BATS 1e), a Hostlag explicit planetary boundary layer formulation, a Kuo-Anthes cumulus parameterization, a modified radiation package (CCM3), as well as chemical, hydrological, and biological processes.

The model has been used to simulate regional climate in East Asia and performs well (Fu et al., 2005; Xiong et al., 2003, 2006, 2009; Xiong, 2004). Xiong et al. (2006) conducted a continuous 10-yr simulation over Asia from 1 July 1988 to 31 December 1998 using RIEMS and found that the model could well reproduce the spatial pattern and seasonal cycle of surface temperature and precipitation as compared with observations. The ability of RIEMS to simulate extreme monsoon rainfall over the Yangtze River valley was examined in the study of Xiong (2004). A continuous 22-yr simulation was also conducted using RIEMS 2.0 in the study of Xiong et al. (2009), the results indicated its ability to simulate the summer monsoon over East Asia.

The chemical aerosol model is coupled online with the climate model (Liu et al., 2010). The distribution of aerosol concentrations calculated by the chemical-aerosol model is passed to the radiation package CCM3 in the climate model to simulate the direct climate effect and, simultaneously, to the cloud parameterization process of the climate model to compute the first indirect climate effect of anthropogenic aerosols using the scheme presented in Hegg (1994).

2.2 Mixing assumptions

Three aerosol species were considered in this study: anthropogenic sulfate, BC, and OC, and three mixing assumptions were made in the simulations: external mixing (EM), internal mixing (IM), and partial internal mixing (IEM) states. Table 1 describes each assumption. The mass ratio of the internal mixture is presented as follows: $R = M_{\rm int}/M$, where R is a parameter independent of particle size in the present study, $M_{\rm int}$ denotes the mass of internal mixture, and M denotes the total mass of aerosols. For the extreme cases of external and internal mixing assumptions, $R = 1$ and $R = 0$, respectively. In the internal mixing assumption, the concentrations of anthropogenic sulfate

and carbonaceous aerosols calculated by the chemical aerosol module were summed as one kind of internally mixed aerosol (IMA). Subsequently, the distribution of IMA was simultaneously passed to the radiation package CCM3 and to the cloud parameterization process of the climate model to compute the indirect radiative forcing effects of IMA.

Table 1. List of experiments

Experiment	Aerosol species	Mass ratio of IMA
BASE	Background aerosols	0
EM	Sulfate, BC, and OC	0
IM	IMA	1
IEM	Sulfate, BC, OC, and IMA	0.5

For the partial internal mixing state, we assumed that halves of the aerosol mass of each aerosol component were internally mixed, so the mass ratio of the internal mixture neither evolved with time nor varied with other factors such as altitude. The mass fraction of the internal mixture was therefore 50% or $R = 0.5$. Consequently, half-masses of sulfate, BC, and OC calculated by the chemical aerosol module were added to substitute for IMA. As mentioned before, the number ratio of internal mixture varies with the size distribution and altitude. Strom et al. (1992) and Fassi-Fihir et al. (1997) found that the number ratio of the internal mixture was approximately 50% on the submicron scale. In the studies of Schwarz et al. (2008) and Vester et al. (2007), the mean value of R of aerosol particles with submicron size was larger than 0.4 although it varied with altitude. Therefore, according to the fact that anthropogenic aerosol particles are generally of submicron size, fixing R at 0.5 is reasonable here.

The morphology of the internal mixture particles in the internal mixing and partial internal mixing assumptions is a core-shell model where the spherical particle is made of two concentric regions: the shell and the core, each with its own uniform refractive index. The optical properties, and specifically the extinction coefficient, single scattering albedo, and asymmetry factor, were calculated by the Mie model for core-shell particles (BHCOAT) developed by Joseph (1993) and based on Bohren and Hoffman (1983). In the BHCOAT code, refractive indices of shell and core required user input. Soluble sulfate was assumed to act as the shell, and the mixture of BC and OC acted as the core in the present study. The sulfate shell had a refractive index of 1.53–0i, while a simple volume average of the individual refractive indices was used to simultaneously compute the refractive index of the BC-OC core in the model, as follows:

$$\begin{aligned} m_{\text{core}} &= \frac{m_{\text{BC}}V_{\text{BC}} + m_{\text{OC}}V_{\text{OC}}}{V_{\text{BC}} + V_{\text{OC}}} \\ &= \frac{R_{\text{BC}}V_{\text{BC}} + R_{\text{OC}}V_{\text{OC}}}{V_{\text{BC}} + V_{\text{OC}}} - \mathrm{i}\frac{I_{\text{BC}}V_{\text{BC}} + I_{\text{OC}}V_{\text{OC}}}{V_{\text{BC}} + V_{\text{OC}}}, \end{aligned}$$

where m_{core} indicates the refractive index of the mixed core of BC and OC, m_{BC} and m_{OC} denote the refractive indices of BC and OC, respectively, and $R_{\text{BC,OC}}$ and $I_{\text{BC,OC}}$ are the real part and image part of the indices, respectively. The refractive indices of BC and OC are 1.56–0.47i and 1.52–0i, respectively.

2.3 Experimental design

The model domain covers East China and its adjacent areas (16.2°–44.1°N, 93.4°–132.4°E) with a horizontal grid size of 60 km. There are 16 vertical layers and the model top is 100 hPa.

This study used 2006 NCEP/NCAR reanalysis data at 6-h intervals as driving fields and boundary conditions for the climate model calculation. The Asia inventory dataset with the reference year of 2006, taken from Zhang et al. (2009b), a study developed in support of NASA's INTEX-B (Intercontinental Chemical Transport Experiment-phase B) mission, was used for the emissions of SO_2, NO_X, CO, NH_3, BC, OC, and VOCs. Emission sectors of this dataset only included anthropogenic emissions and accounted for power plants, industry, residential, and transportation. The grid size of the dataset is 0.5 degrees.

We conducted four model runs (BASE, EM, IM, and IEM) as listed in Table 1, which span the period from 1 January to 31 December 2006. The simulation results spanning from 11 January to 31 December 2006 were analyzed. The control run (BASE) only contained background aerosols without any anthropogenic aerosols. EM treated anthropogenic sulfate and carbonaceous carbon aerosols as a complete external mixture, whereas IM treated aerosols as a complete internal mixture. In the IEM experiment, 50% of the

aerosol mass was considered to be internally mixed.

3. Model simulation and results

3.1 Distributions of aerosols under different mixing assumptions

Figure 1 shows the distributions of annual average sulfate column burden for the cases of EM, IM, and IEM. The large column burden mainly occurred over East China, but there was also some sulfate concentrated in the atmosphere over the ocean adjacent to the east coast of China, indicating that the sulfate or SO_2, precursor of sulfate was transported by wind to the ocean. The regions with a larger column burden of sulfate were the Sichuan basin, Hunan, Jiangxi, and Zhejiang provinces, located south of the Yangtze River. The column burden of sulfate was generally larger than 20 mg m^{-2} in these regions, with a maximum of 38.9 mg m^{-2} for the EM case. The column burden in the IM case was larger than the EM case, and it was especially significant in regions where sulfate was highly concentrated. The maximum value in the IM case was 79.5 mg m^{-2}, almost twice that of the EM case. The maximum value in the IEM case was 61.5 mg m^{-2}. The regional average column burdens of sulfate for EM, IM, and IEM were 6.15, 11.49, and 10.29 mg m^{-2}, respectively.

The mean column burden of sulfate presented here was generally larger than the global average simulated by the GCM models presented in the studies of Ghan et al. (2001), Kiehl et al. (2000), and Jacobson (2001a), which ranged from 2.33 to 4.0 mg m^{-2}. In those previous studies, East Asia was a region with an obviously high sulfate concentration. The mean column burdens of sulfate in East Asia simulated by other regional climate models were also much greater

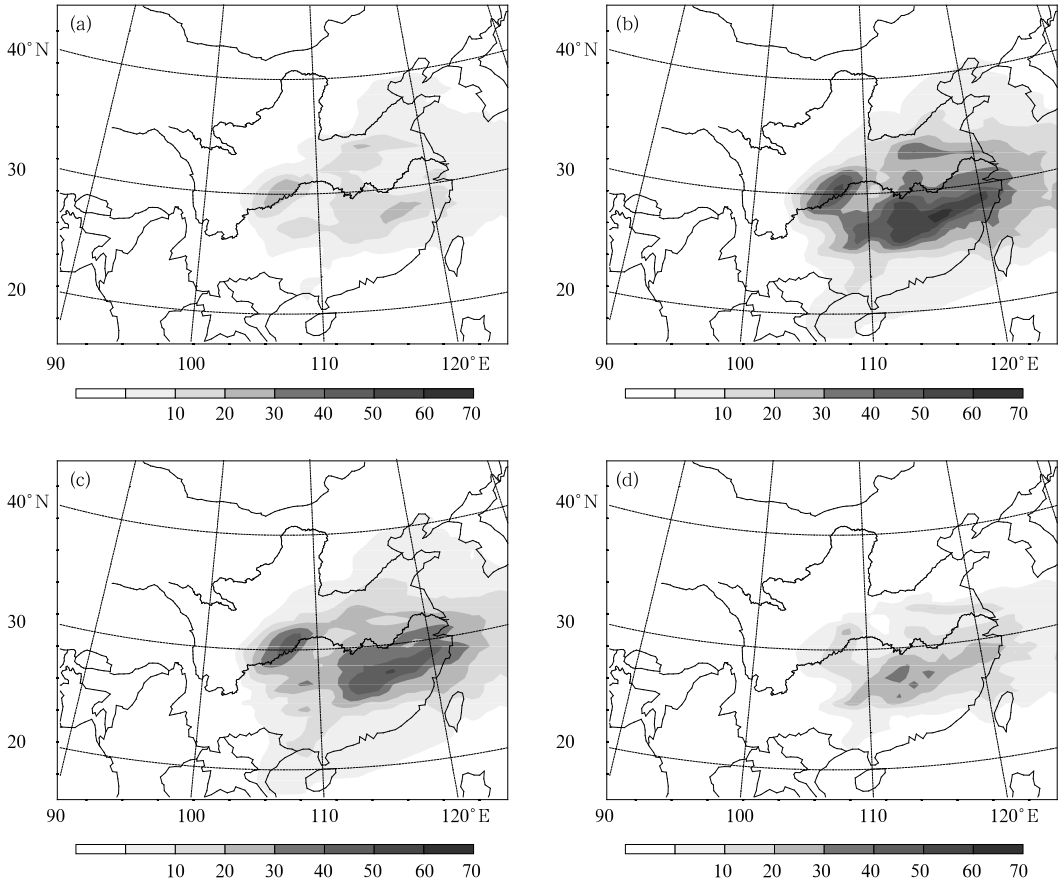

Fig. 1. The annual mean column burden (mg m^{-2}) of sulfate for (a) EM, (b) IM, and (c) IEM cases, and (d) IM–EM. IM–EM denotes the difference between IM and EM.

than the global average value. For instance, Zhang et al. (2009a) found that the mean column burden of sulfate over East Asia was as much as 20 mg m^{-2}, and Qian et al. (2003) found that the mean column burden over China was 17 mg m^{-2}. The regional average column burden for the IM case in this study was closer to the results of Zhang et al. (2009a) and Qian et al. (2003) than to those of the EM case.

It is noteworthy that the mean concentrations of sulfate for EM, IM, and IEM were distinctly different. The mean concentration of sulfate for the IM case or the IEM case was larger than that for the EM case, which was consistent with previous studies. Kim et al. (2008) found that when internal mixtures were included in the model, the total mass of sulfate was increased from 0.72 to 0.80 Tg. Lu and Bowman (2010) used a detailed aerosol mixing state model to simulate the concentrations of multicomponent aerosols and found that both the mass concentration and the number concentration of sulfate in the internal mixing mode are larger than those in the external mode. The increase in sulfate presented here may have been caused by a discrepancy of meteorological conditions as a result of different mixing assumptions made in the simulations. Sulfate was considered to be sensitive to meteorological conditions such as temperature and precipitation. Liu et al. (2007) showed very large differences of the simulated aerosol fields when driving the same aerosol module with different meteorological datasets, including those of the finite-volume general circulation model (FVGCM), the NASA Goddard Global Modeling and Assimilation Office (GMAO), and the NASA Goddard Data Assimilation Office (DAO). Sulfate with FVGCM was 40% less than with DAO, due to greater levels of precipitation.

Figures 2 and 3 show the annual column burden of BC and OC, respectively. As seen in Fig. 2, BC was also mainly centralized in East China, with the highest concentrations occurring in the Sichuan basin and Shanxi Province. The column burdens of BC in the Sichuan basin and Shanxi were larger than 2.1 mg m^{-2}, with maxima of 2.8 (EM) and 3.0 mg m^{-2} (IM). The large amount of the fossil fuels consumed in North China, especially in Shanxi Province, produced high concentrations of BC there. The large concentration occurring in Sichuan was mainly due to the topographical effect of the basin.

The OC distribution pattern, shown in Fig. 3, was similar to that of BC as a result of the homology of BC and OC. Usually, BC and OC are emitted into the atmosphere simultaneously. BC is produced from the insufficient combustion of biomass or fossil fuels, while OC is produced by the complete combustion and the conversion of volatile organic compounds and hydrocarbon chemical reactions. The column burden of OC was larger than that of BC by a factor of 3 to 5 over the domain. The column burden of OC was larger than 4.0 mg m^{-2} in Shanxi Province and larger than 7.5 mg m^{-2} in the Sichuan basin, with a maximum of 8.3 mg m^{-2} for IM. BC and OC were also concentrated over the ocean, indicating the long-distance transport of carbonaceous aerosols.

The patterns of BC and OC in the present study were consistent with those in previous studies (Qian et al., 2001, 2003; Han et al., 2008; Zhang et al., 2009a). Han et al. (2008) simulated the distributions of carbonaceous aerosols by use of coupled regional climate models and indicated that BC and OC were mainly concentrated in the Sichuan basin, the lower reaches of Yangtze River, and Shanxi Province. Zhang et al. (2009a) found similar results by using a global climate model.

The distributions of BC and OC are almost the same in EM, IM, and IEM. Figures 2 and 3 show the differences between IM and EM and point to slight increases in both BC and OC over the Huanghai Sea. BC and more than half of OC compounds are emitted directly from the source and are considered primary aerosols. The distributions and concentrations of these primary aerosols are mainly affected by atmospheric circulation instead of temperature and precipitation. BC and OC are therefore much less sensitive to temperature and precipitation than sulfate. The mean column burdens of BC and OC for EM, IM, and IEM suggest slight discrepancies due to mixing assumptions and are shown in Table 2.

The annual mean column burdens of BC and OC over the domain were 0.462±0.008 and 2.162±0.07 mg m^{-2}. Additionally, the average column burden of primary OC was 1.256±0.018 mg m^{-2} while that of secondary OC was 0.896±0.001 mg m^{-2}. Qian et al. (2003) concluded that the mean column burdens

of BC and OC were 0.8 and 8 mg m^{-2} over East Asia, respectively. Han et al. (2008) showed that the column burdens of BC were approximately 4–8 and 8–12 mg m^{-2} in the regions where the carbonaceous aerosols were highly concentrated. Zhang et al. (2009a) found that the column burden of OC was as much as 10 mg m^{-2} in the Sichuan basin. When compared with previous results, however, the results in this study presented smaller column burdens of carbonaceous aerosols. This is due to the exclusion of nature biomass emissions in this study in exchange for a focus solely on anthropogenic emissions.

The ratio of OC burden to BC burden was approximately 4.6, a result consistent with Zhang et al. (2009a), which indicated that the mean column burden of OC was larger than that of BC by a factor of 4.0. The surface concentrations of BC and OC were 1.045±0.5 μg m^{-3} and 2.24±0.03 μg m^{-3}, respectively. The OC/BC ratio was 2.14±0.02, similar to the results of Novakov et al. (2005), which analyzed the published data of observations in China indicating an OC/BC ratio of 2.39±0.47.

Table 2 lists the regional average column burdens of sulfate, BC, POC, SOC, and total OC. The disparity in BC was less than 4% and 1% in OC. In contrast, the disparity in sulfate was much larger.

Table 2. Average column burden of anthropogenic aerosols (mg m^{-2})

	EM	IM	IEM
Sulfate	6.145	11.494	10.291
BC	0.453	0.470	0.468
POC	1.259	1.274	1.264
SOC	0.896	0.895	0.898
OC	2.155	2.169	2.162

Note: black carbon (BC), primary organic carbon (POC), secondary organic carbon (SOC), and organic carbon (OC).

3.2 Comparison of modeled aerosol concentrations with observations

Prior to this study, observations of the surface concentrations of sulfate or carbonaceous aerosols were

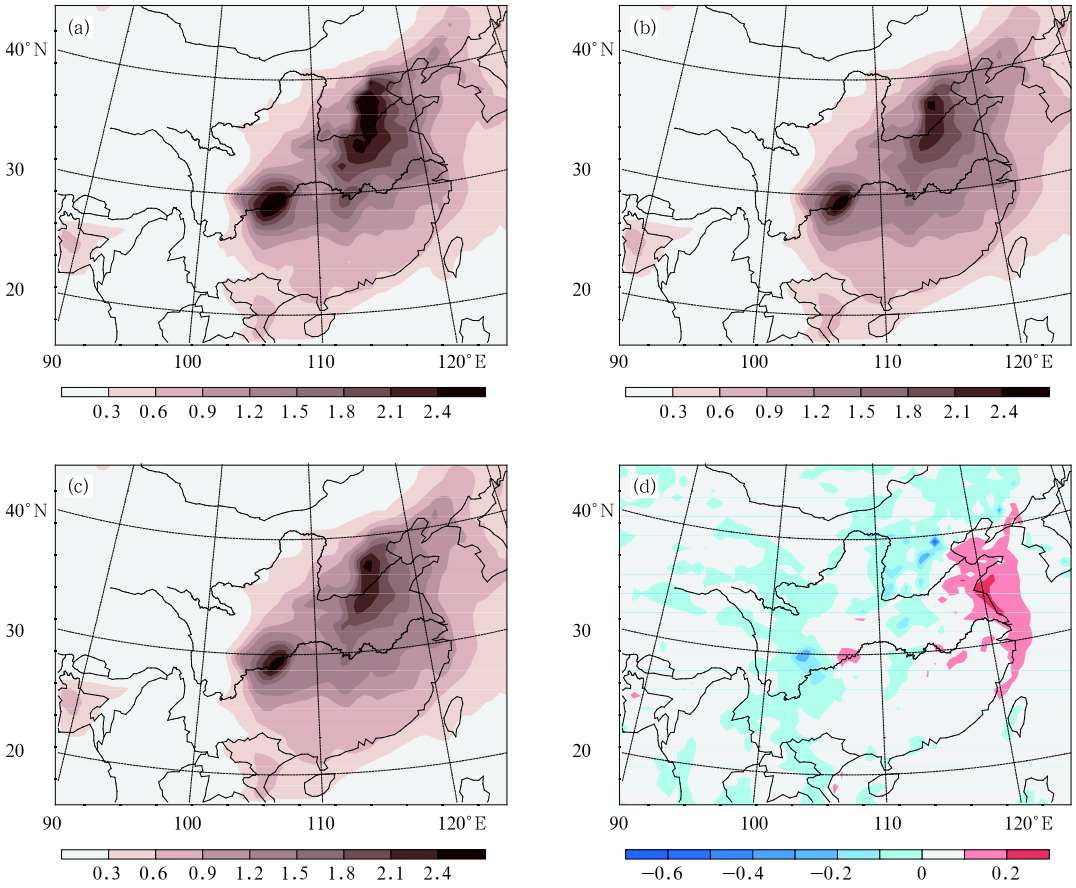

Fig. 2. As in Fig. 1, but for BC (mg m^{-2}).

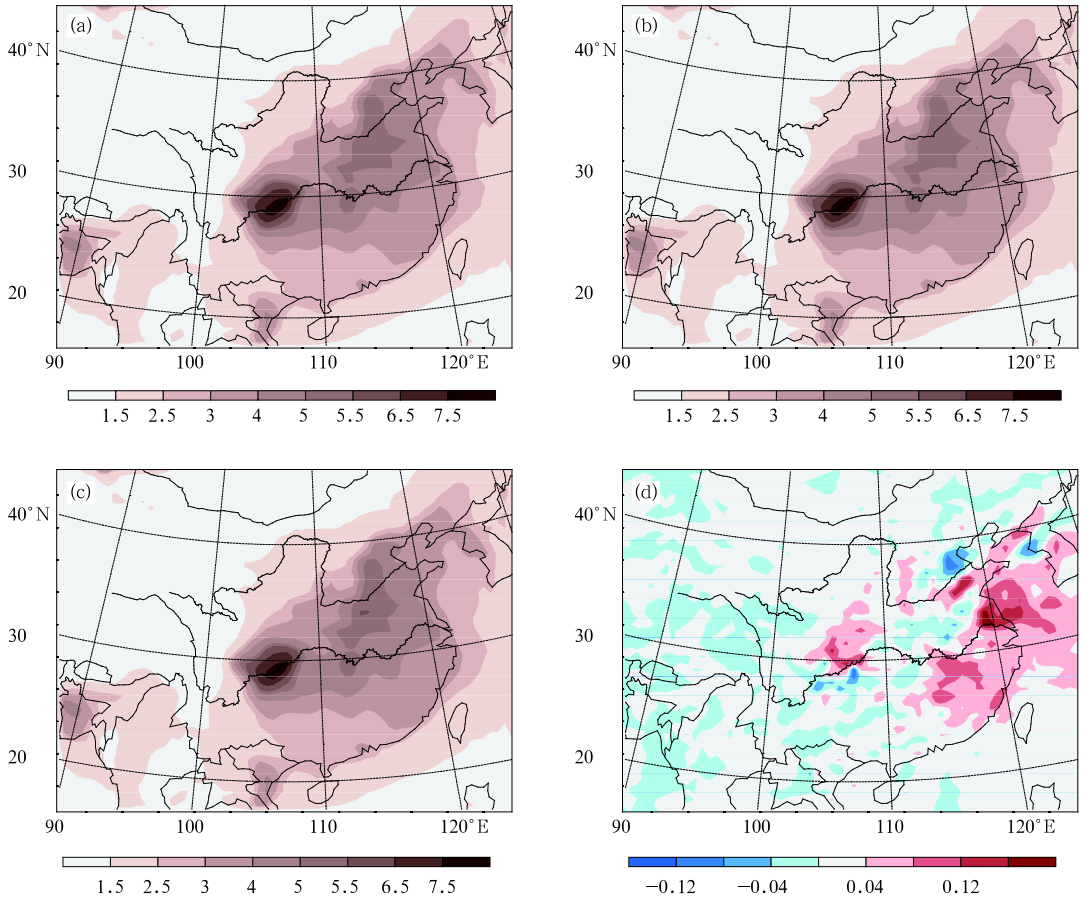

Fig. 3. As in Fig. 1, but for OC (mg m^{-2}).

still limited in East Asia. In this study, measurements of sulfate and carbonaceous aerosol concentrations at a variety of locations in East Asia were collected, as shown in Table 3. The observations presented here were conducted in 25 cities in China and 3 cities in Korea. These measurements were carried out in or around 2006. Table 3 shows that observations were higher than modeled results at most measurement sites. The model always underestimated the surface concentrations because of the exclusion of natural sources of sulfate and carbonaceous aerosols in this study. Nevertheless, the modeled results agreed with observations in magnitude over the majority of the measurement sites. For locations with high altitudes like Lhasa (3663 m), Dunhuang (1139 m), Lanzhou (2057 m), and Zhengbeitai (1135 m), the model underestimated the surface concentrations by a factor of 101 to 102. The observation of Lhasa was conducted in a measurement site located in the downtown area, which covers only 60 km^2. The observed concentrations could not, therefore, be replicated by a cell average of the model with the grid size of 60 km. The Dunhuang, Lanzhou, and Zhengbeitai sites were rural. The mean variances of BC mass concentrations between simulated results and observations were 45% (EM) and 43% (IM). For OC, the variances were 59% for both EM and IM. The discrepancies for sulfate were smaller than for carbonaceous aerosols, which were 36% (EM) and 28% (IM). In sum, the simulated results for IM were somewhat closer to the observations than EM results.

3.3 Optical depth of aerosols under different mixing assumptions

Satellite instruments, such as the Moderate Resolution Imaging Spectroradiometer (MODIS) and the

Table 3. Observed and simulated (EM and IM) aerosol mass concentrations (μg m^{-3})

Location	Sulfate			BC			OC			Measurement	Reference
	Obs	EM	IM	Obs	EM	IM	Obs	EM	IM	period	
Chengdu(30°39′N, 104°2.4′E)	/	37.36	28.84	11.1	7.38	4.87	33.4	13.93	14.36	2006	Zhang et al., 2008
Dalian(38°54′N, 121°37.8′E)	/	7.14	7.52	5.3	3.41	3.25	17.7	5.46	5.36	2006	Zhang et al., 2008
Dunhuang(40°9′N, 94°40.8′E)	/	0.2	0.19	4.1	0.05	0.03	29.3	0.26	0.26	2006	Zhang et al., 2008
Gaolanshan(36°0′N, 105°51′E)	/	2.96	2.95	3.7	1.59	1.31	18.2	2.69	2.68	2006	Zhang et al., 2008
Gucheng(39°7.8′N, 115°48′E)	/	15.34	17.81	12	6.24	5.84	42.2	8.64	8.53	2006	Zhang et al., 2008
Jinsha(29°37.8′N, 114°12′E)	/	13.54	13.85	3.2	3.17	3.24	14.3	5.58	5.66	2006	Zhang et al., 2008
Lhasa(29°40′N, 91°7.8′E)	/	0.12	0.12	3.7	0.08	0.05	21	0.18	0.18	2006	Zhang et al., 2008
Lin'an(30°18′N, 119°44′E)	/	15.08	13.64	4.80	4.53	4.62	14.90	7.64	7.67	2006	Zhang et al., 2008
Nanning(22°49′N, 108°21′E)	/	6.15	6.03	3.70	1.50	1.33	15.30	3.35	3.33	2006	Zhang et al., 2008
Panyu(23°0′N, 113°21′E)	/	15.40	10.07	9.30	3.99	2.39	21.00	6.85	6.79	2006	Zhang et al., 2008
Changde(29°10.2′N, 111°42.6′E)	/	10.23	12.01	2.30	3.48	3.35	11.1	8.62	8.70	2006	Zhang et al., 2008
Xi'an(34°25.8′N, 108°58.2′E)	/	20.40	11.87	14.20	4.54	2.99	42.8	5.49	5.63	2006	Zhang et al., 2008
Zhengzhou(34°47′N, 113°41′E)	/	16.13	16.68	9.40	7.73	6.82	25.3	10.47	10.52	2006	Zhang et al., 2008
Taiyuan(37°52′N, 112°34′E)	/	25.28	15.37	4.70	9.22	6.54	18.60	10.72	10.75	2006	Meng et al., 2007
Lanzhou(36°08′N, 103°41′E)	9.8	0.21	0.21	/	0.06	0.06	/	0.20	0.21	2006	Pathak et al., 2009
Daihai(40°37′N, 112°35′E)	/	4.43	4.87	3.10	1.93	1.66	19.9	2.8	2.79	2005–2007	Han et al., 2008
Deokjeok (37°13′N, 126°9′E)	6.00	2.96	3.6	1.00	0.81	1.16	3.80	1.53	1.58	2005–2007	Kim et al., 2009
Gosan (33°17′N, 126°10′E)	6.00	2.60	3.16	0.80	0.57	0.88	2.70	1.21	1.19	2005–2007	Kim et al., 2009
Zhuzhang(28°00′N, 99°43′E)	1.60	1.40	1.46	0.34	0.12	0.17	3.10	1.74	1.75	2004–2005	Qu et al., 2009
Hongkong(22°16′N, 114°10′E)	8.69	8.42	6.99	2.14	1.44	1.34	4.25	3.43	3.44	2004–2005	So et al., 2007
Zhenbeitai(38°26′N, 109°12′E)	/	1.31	1.84	4.00	0.49	0.52	11.90	0.94	0.97	2004–2005	Zhang et al., 2008
Shangdianzi(40°39′N, 117°07′E)	/	6.9	7.35	2.5	2.92	3.28	10.40	4.51	4.46	2004–2005	Zhang et al., 2008
Beijing(39°48′N, 116°28′E)	26.30	28.75	16.15	5.40	12.45	6.87	31.30	12.86	12.64	2004	Xie et al., 2008
Guangzhou(23°8′N, 113°16′E)	27.80	15.40	10.10	7.10	4.00	2.40	22.40	6.90	6.80	2004	Andreae et al., 2008
Seoul(37°30′N, 127°00′E)	5.77	4.68	2.97	2.91	3.65	1.93	9.45	6.41	6.43	2003–2006	Heo et al., 2009
Taipei(25°02′N, 121°26′E)	6.40	4.21	6.84	1.60	1.49	1.72	5.00	3.56	3.64	2002–2008	Chang et al., 2010
Beijing(39°48′N, 116°28′E)	18.46	28.75	16.15	/	12.45	6.87	/	12.86	12.64	2001–2006	Okuda et al., 2008
Hangzhou(30°16′N, 120°09′E)	20.10	15.08	13.64	4.06	4.53	4.62	21.41	7.64	7.67	2001–2002	Cao et al., 2009
Beijing(39°48′N, 116°28′E)	14.64	28.75	16.15	9.40	12.45	6.87	25.30	12.86	12.64	1999–2000	He et al., 2001
Shanghai(31°14′N, 121°28′E)	14.02	11.29	15.02	6.49	5.04	5.43	14.89	9.62	9.69	1999–2000	Ye et al., 2003
Hongkong(22°16′N, 114°10′E)	/	8.42	6.99	4.66	1.44	1.34	8.89	3.43	3.44	1998–2001	Yu et al., 2004

Slash denotes that no observation is available for reference.

Multi-angle Imaging Spectroradiometer (MISR), and ground-based instruments, such as aerosol lidar, have been used to measure the total aerosol optical depth (AOD). Anthropogenic AOD could not be directly derived from these measurements because they also include natural source. Estimates of the anthropogenic AOD were therefore predominately based on numerical models as suggested by Yu et al. (2006). The distributions of AOD (at 550 nm) due to anthropogenic sulfate and carbonaceous aerosols in three different cases, as well as the pattern of AOD differences between IM and EM, were illustrated in Fig. 4. As can be seen, AODs were higher in eastern China and the Sichuan basin where anthropogenic aerosols were highly concentrated in different cases. The AOD in the IM case was larger than that in the EM case over the simulated region, due primarily to the higher concentration of sulfate in IM than that in EM. The annual averages of AOD for IM, IEM, and EM were 0.109, 0.096, and 0.063, respectively. The average AODs over East Asia calculated by RIEMS 2.0 were larger than those computed by the global models, as listed in Table 3. However, the AOD results using only anthropogenic sulfate and carbonaceous aerosols as presented in this study were smaller than those derived from satellite and ground-based observations, such as MODIS and the Aerosol Robotic Network (AERONET) data, which were, comparatively, contributed by total aerosols, presented in the studies of Adhikary et al. (2008), Yu et al. (2006), and Chung et al. (2010). The results in Yu et al. (2006) showed that the annual average AOD was about 0.14 over

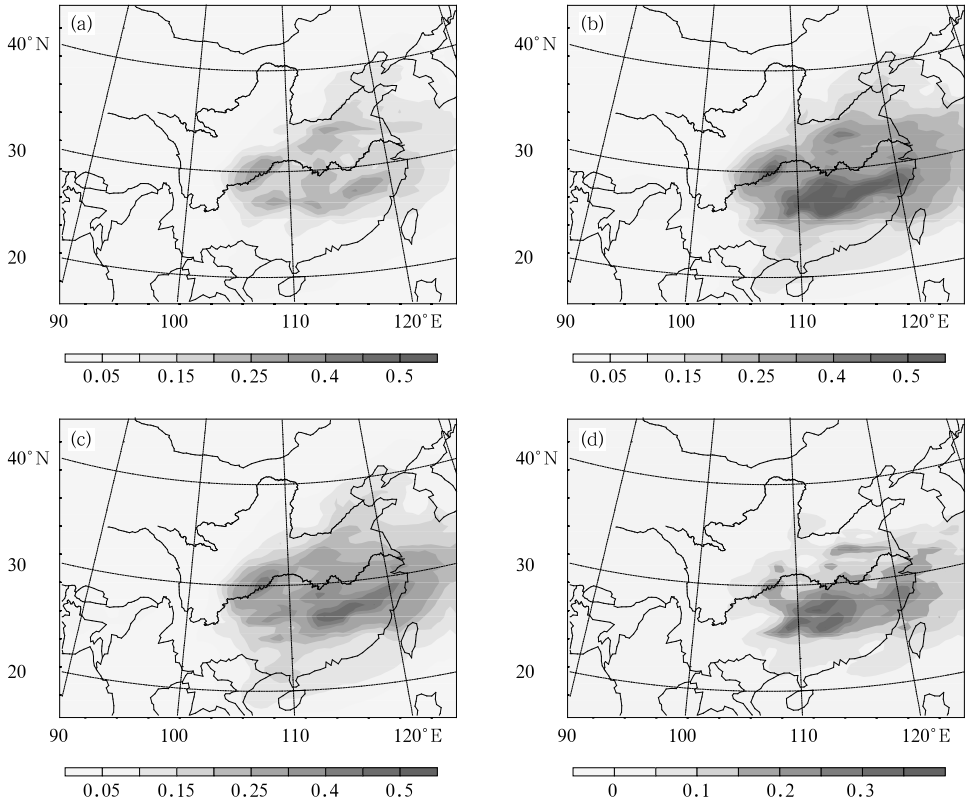

Fig. 4. Aerosol Optical Depth (AOD) for (a) EM, (b) IM, and (c) IEM cases, and (d) IM–EM. IM–EM denotes the difference between IM and EM.

global ocean derived from MODIS, whereas the annual average AOD over global land derived from MISR was about 0.23. The fraction of anthropogenic AOD was about 47%±9% over land and 21%±7% over ocean. Consequently, the anthropogenic AOD could be derived as 0.11±0.02 over global land and 0.03±0.01 over global ocean, respectively. Zhou et al. (2005) showed the mean values of AERONET AOD at 550 nm as 0.25 over East Asia for fine-mode aerosols, which can be a surrogate for deriving anthropogenic AODs because anthropogenic aerosols are predominantly submicron in size. A qualitative rather than quantitative comparison between AOD simulations and observations was made in this study.

Chung et al. (2010) assimilated MODIS AOD and AERONET AOD data for the period 2001–2004 and found that East China and the Sichuan basin were the regions with the highest AODs. Similar results were also presented in the study of Adhikary et al. (2008) using the mean MODIS AOD data with AERONET corrections. The distributions of AOD shown in Fig. 4 generally followed those patterns in Chung et al. (2010) and Adhikary et al. (2008) in East Asia, with smaller AOD values by a factor of 2. Additionally, the simulated patterns and AOD values were consistent with the simulation results in Huang et al. (2007) and Chung et al. (2010). Huang et al. (2007) simulated the AOD of anthropogenic sulfate and carbonaceous aerosols and found that the AOD was maximized over the Sichuan basin and exhibited a broad region of over 0.3 extending to northeastern China. The anthropogenic AODs contributed by anthropogenic sulfate and carbonaceous aerosols were simulated by Chung et al. (2010) using the integrated MODIS and AERONET data and were about 0.4–0.5 over the Sichuan basin and 0.35–0.45 over East China, which were similar to the results of this study.

3.4 Radiative forcing of aerosols under different mixing assumptions

As Kim et al. (2008) suggested, the mixing assumption was one of the major factors causing

different estimates of the total radiative forcing (RF) when more than one aerosol component was introduced into the model. Some previous studies have investigated the variation between the external and internal mixing assumptions (Haywood and Shine, 1995; Jacobson, 2001a; Lesins et al., 2002; Stier et al., 2006; Schwarz et al., 2008) and found that the surface RF was decreased dramatically when BC was internally mixed. Lesins et al. (2002) and Schwarz et al. (2008) suggested that the absolute value for RF at the top of the atmosphere caused by the external mixture of sulfate and BC was larger than that caused by an internal mixture. Using offline climate models or conceptual radiative models, these studies have focused on the variations in the optical properties of aerosol mixtures but ignored variations in aerosol mass. The RF values would also vary with the aerosol mass concentrations predicted by the aerosol model. Lesins et al. (2002) suggested that studies applied to predicting aerosol mass concentrations from general circulation models were needed to quantify the influence of the mixing assumptions on the RF and its implications for the anthropogenic influence more reliably. In the present study, we overcome these shortcomings with an online coupled aerosol-climate model.

This study considered both direct and indirect radiative forcing. The radiative forcing here was under an all-sky condition at the top of the atmosphere if not with any additional explanation. Figure 5 shows the distribution of the annual mean RF values due to anthropogenic sulfate and carbonaceous aerosols at the top of the atmosphere (TOA). The patterns of radiative forcing for different simulating cases were closely consistent with those of AOD and were similar to the burdens of aerosols. The RF at TOA was negative over the domain with extreme values of –4.61, –8.15,

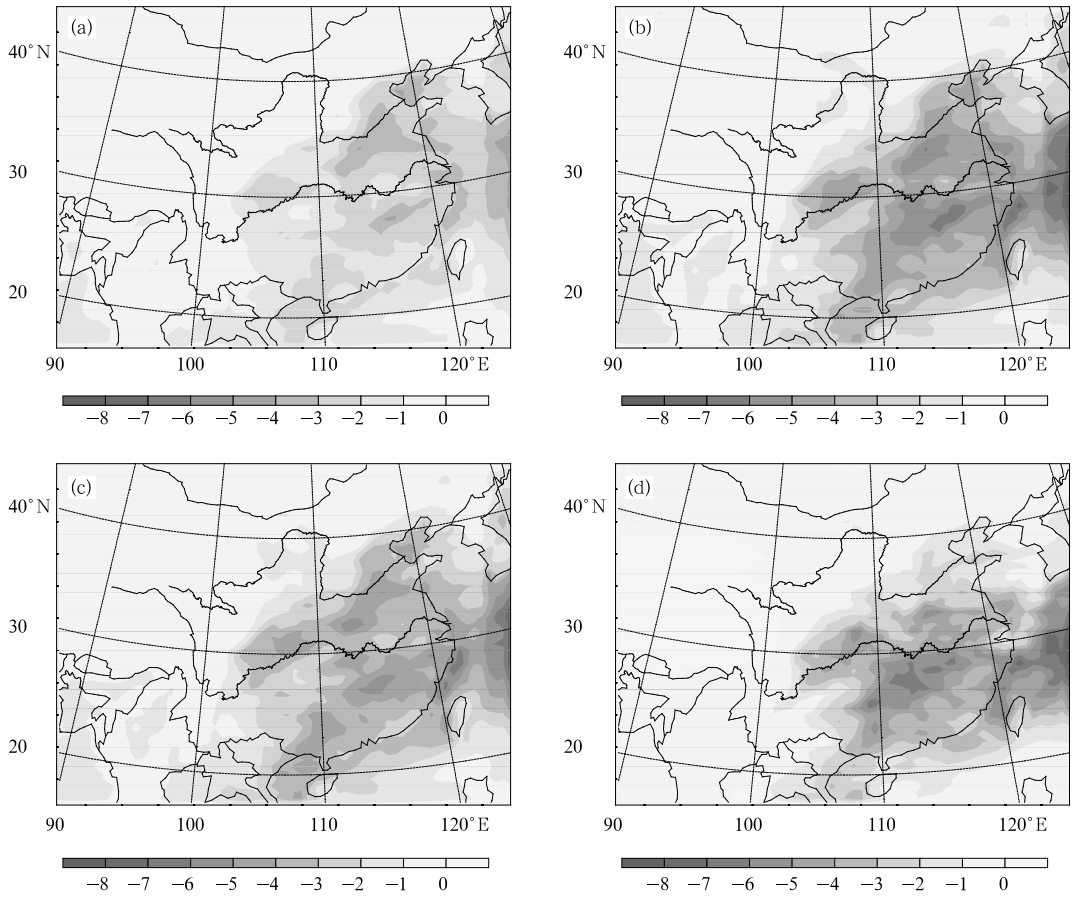

Fig. 5. Radiative forcing (W m^{-2}) at the TOA for (a) EM, (b) IM, (c) IEM cases, and (d) IM–EM. IM–EM denotes the difference between IM and EM.

and –7.12 W m^{-2} for EM, IM, and IEM, respectively, suggesting that it would result in global cooling as a sum in either EM or IM. The magnitude of RF in the IM case was always larger than that in EM across the domain. The annual mean values for IM, IEM, and EM were –1.97, –1.82, and –1.27 W m^{-2}, respectively.

The impacts of relative humidity on the optical properties of aerosols were taken into consideration in RIEMS 2.0. This consideration consequently resulted in large negative RF values over the ocean adjacent to the east coast of China due to high relative humidity in that region. Penner et al. (1998) found an increase in the RF of sulfate due to a decrease in relative humidity. When the humidity was restricted to lower than 90%, the mean RF increased from –0.81 to –0.55 W m^{-2}.

Figure 6 shows the monthly mean values of RF for EM, IM, and IEM. July and May were the months with the highest RF values: –4.03 W m^{-2} in July and –3.49 W m^{-2} in May for IM. The values and variations of RF were lower in autumn and winter. Larger RF values resulting from internal mixtures rather than external mixtures appeared in most months.

The variations of RF between IM and EM were negative over the whole domain. As can be seen in Figs. 1 and 5, the pattern of the difference in RF between IM and EM was similar to that of sulfate burden. Such a similarity in pattern implied that changes in sulfate burden may cause changes in RF values.

As described in the fourth Assessment Report of the Intergovernmental Panel on Climate Change (IPCC, 2007), the global average estimates of direct and indirect RF of anthropogenic aerosols were –0.1 to approximately –0.9 W m^{-2} and –0.3 to approximately –1.8 W m^{-2}, respectively. Previous modeled results and observations showed that the RF due to anthropogenic sulfate and carbonaceous aerosols was larger than –1 W m^{-2} over East Asia (Penner et al., 1992; Hansen et al., 2002; Giorgi et al., 2003; Chung et al., 2005; Schulz et al., 2006; Huang et al., 2007). Giorgi et al. (2003) estimated that the direct radiative forcing due to sulfate over China was –7 to approximately –1 W m^{-2} and that the sums of direct forcing and indirect forcing were up to –3.93 W m^{-2} in winter and –11.77 W m^{-2} in summer over East China. It further indicated that the sums of direct and indirect forcing reached up to –7.02 W m^{-2} in winter and –10.52 W m^{-2} in summer over the Sichuan basin. Chung et al. (2005, 2010) also obtained a similar result, which indicated that the absolute value of RF was higher than –2 W m^{-2} over most regions of East Asia due to anthropogenic aerosols. The annual mean RF over East China reached up to –6 W m^{-2}. Huang et al. (2007) showed that anthropogenic aerosol RF was –1.91 to approximately –1.41 W m^{-2} on average over East Asia. The results in the present study were consistent with these estimates.

In Table 4, we compared the burdens of total anthropogenic aerosol, RF at TOA, and normalized radiative forcing (NRF) simulated by eight AeroCom global models (Schulz et al., 2006), four regional models (Chang and Park, 2004; Chung et al., 2010; Huang et al., 2007; Wu et al., 2005), and the RIEMS 2.0 under different mixing assumptions. The AeroCom global models and two regional models used by Chung et al. (2010) and Huang et al. (2007) were coupled with detailed aerosol modules, including anthropogenic sulfate, BC, and OC, to simulate the direct and indirect effects of these aerosols. While Chang and Park (2004) simulated the direct effect of anthropogenic aerosols and sea salt, Wu et al. (2005) only simulated the direct effect of sulfate. Table 4 shows that the average global burdens of anthropogenic aerosols, as simulated by global models, were always less than the burden modeled by RIESM 2.0 over East Asia. Additionally, the RF results of those global models were less than

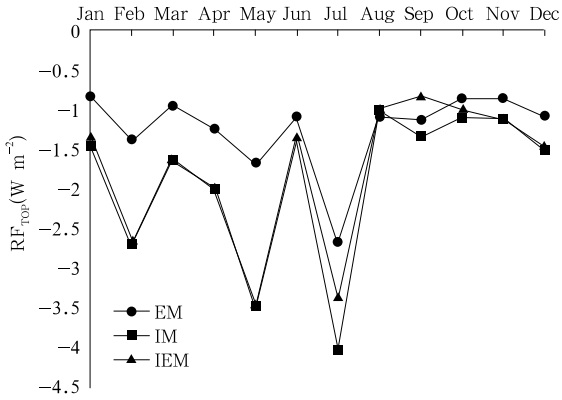

Fig. 6. Monthly average of radiative forcing at the TOA (W m^{-2}) for EM, IM, and IEM cases.

Table 4. Simulated burden of total anthropogenic sulfate and carbonaceous aerosols (mg m^{-2}), radiative forcing (W m^{-2}) at TOA and normalized radiative forcing (NRF) (W mg^{-1}) from 8 global models, 4 regional models, and the RIEMS 2.0 model under different mixing assumptions in this study

Model	Load (mg m^{-2})	AOD	RF at TOA (W m^{-2})	NRF (W mg^{-1})	Reference
LOA	6.0	0.049	–0.09	–0.02	Reddy and Boucher, 2004
GISS	2.8	0.014	–0.11	–0.04	Schulz et al., 2006
UIO GCM	2.7	0.021	–0.11	–0.04	Kirkevag and Iversen, 2002
GATORG	6.4	/	–0.12	–0.02	Jacobson, 2001a
MPI HAM	3.4	0.032	–0.27	–0.08	Schulz et al., 2006
UMI	4.0	0.028	–0.41	–0.10	Schulz et al., 2006
LSCE	4.8	0.033	–0.28	–0.06	Schulz et al., 2006
ULAQ	3.7	0.030	–0.24	–0.06	Schulz et al., 2006
RegCM2	/	0.149	–4.57	/	Huang et al., 2007
PNNL-STEM-MARK	/	/	–1.3	/	Chung et al., 2010
MM5	20	/	–4.1	–0.22	Chang et al., 2004
RegCM2	2.42	/	–0.38	–0.16	Wu et al., 2005
RIEMS(EM)	8.75	0.063	–1.27	–0.145	This study
RIEMS(IM)	14.13	0.109	–1.97	–0.139	This study
RIEMS(IEM)	12.92	0.096	–1.82	–0.141	This study

Note that Chang et al. (2004) simulated the direct effect of anthropogenic aerosols and sea salt, and Wu et al. (2005) simulated direct effect of sulfate.

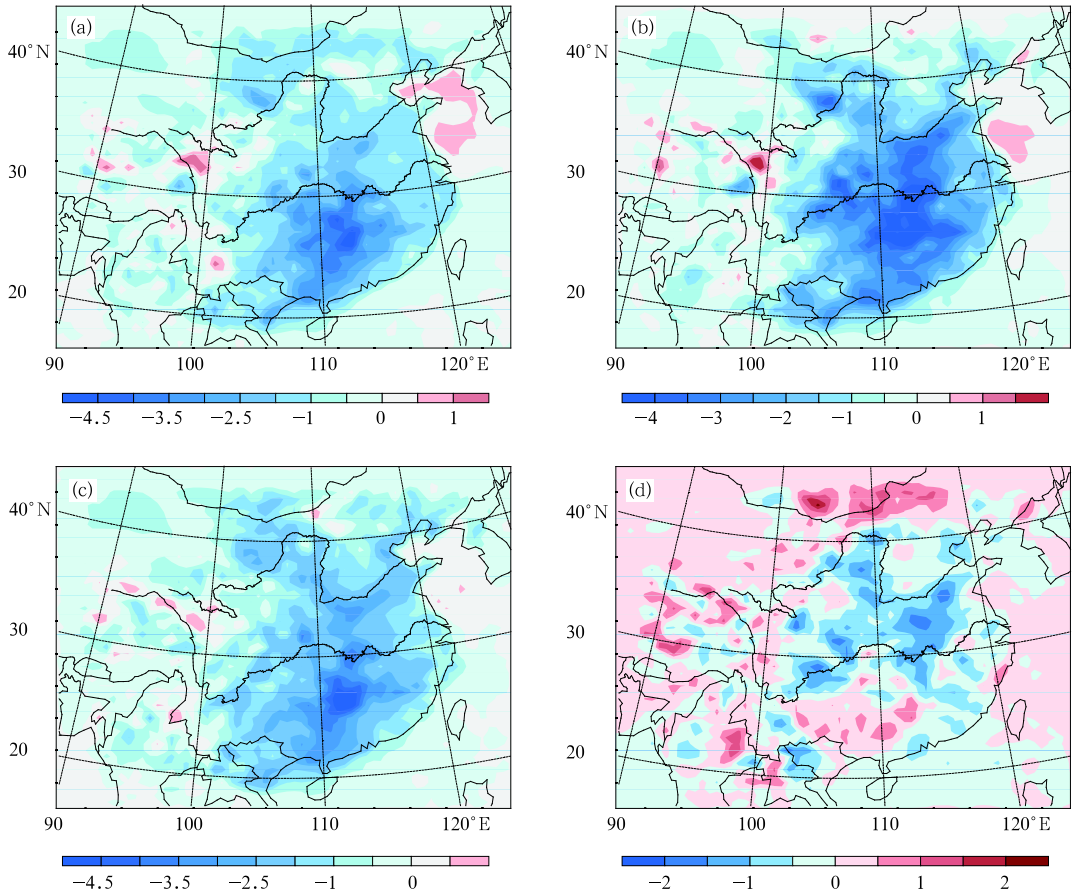

Fig. 7. Annual surface air temperature changes (10^{-1} K) for (a) EM, (b) IM, and (c) IEM cases, and (d) IM–EM. IM–EM denotes the difference between IM and EM.

that of RIEMS 2.0 by a factor of 3 to 20. When considering the NRF, the results presented in this study were consistent with those in previous studies listed in Table 4. The values of NRF ranged from –0.02 to –0.10 W mg^{-1} for different global models, always being smaller than the NRF obtained by RIEMS 2.0. The RIEMS 2.0 NRF results were –0.145, –0.139, and –0.141 W mg^{-1} for EM, IM, and IEM, respectively. However, the NRFs for EM, IM, and IEM were consistent with the results of other regional models, as shown in Table 4. The NRF of IM was less than that of EM, which was consistent with the results in Lesins et al. (2002). That study suggested that the NRF of an internal mixture was less than that of an external mixture, but the result presented here is smaller than that of Lesins et al. (2002).

3.5 Climate effects of aerosols under different mixing assumptions

Figure 7 illustrates the annual mean changes in surface temperature due to aerosols. The regions with significant changes in surface temperature were the middle and lower reaches of the Yellow and Yangtze Rivers and North China. The variations exceeded 0.25 K in these regions, with maxima of –0.47 K (EM), –0.49 K (IEM), and –0.50 K (IM). The temperature differences between IM and EM primarily occurred in the regions between the Yellow and Yangtze Rivers. The temperature in IM was lower than in EM in these regions, but the opposite occurred over the southwest and northwest regions of China and Mongolia. Regions of significant changes in surface temperature did not exactly correspond to the regions of RF, indicating the complexity of aerosol impacts on climate.

Figure 8 displays the impact of anthropogenic aerosols on annual precipitation. It is apparent that the total area size of regions with decreases in precipitation is larger than that of regions with precipitation increases. There were obvious decreases in a band-shaped region of Guizhou, Chongqing, Hunan,

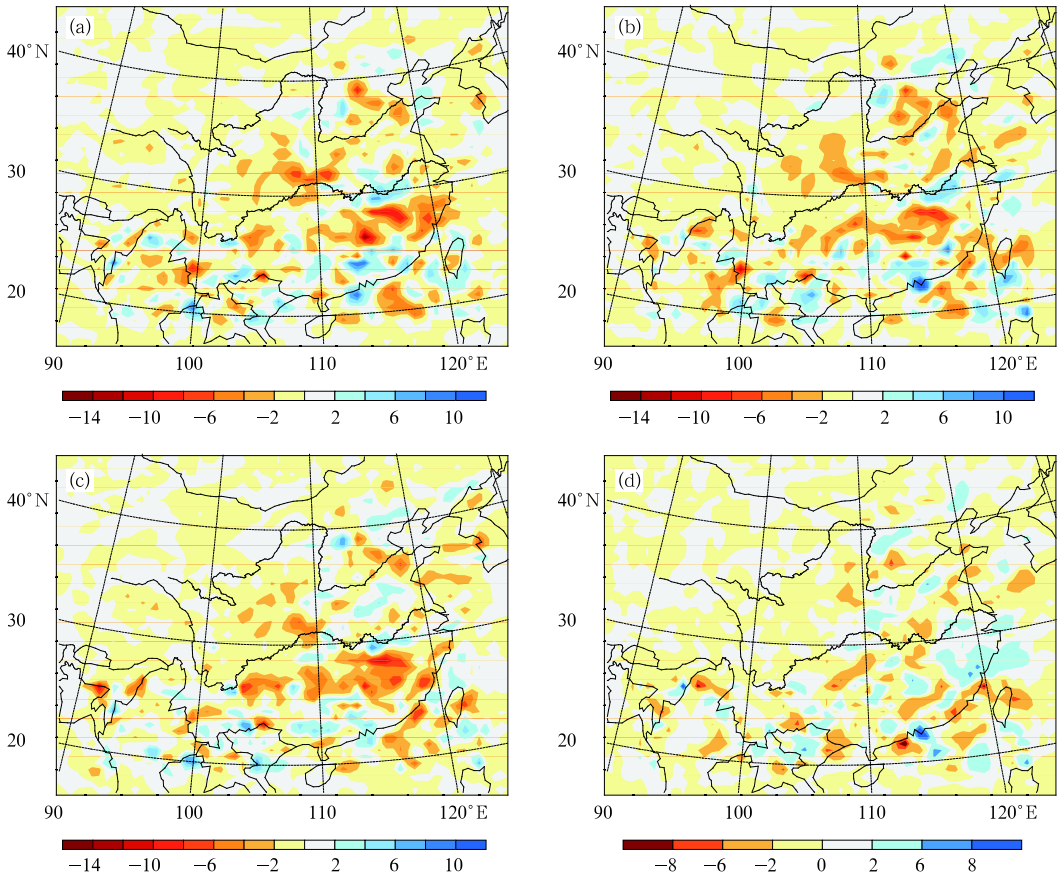

Fig. 8. As in Fig. 7, but for annual precipitation changes (10 mm).

Jiangxi provinces, south of the Yangtze River. The precipitation reductions in these regions reached 40 mm, with maxima of 148, 122, and 102 mm for EM, IM, and IEM, respectively, showing a significant decrease in Jiangxi Province where temperatures also decreased remarkably. Conversely, precipitation increased in some parts of South and North China, including Shanxi and Guangdong provinces for both EM and IM.

In this study, we analyzed the climate effects due to anthropogenic aerosols in four climate sub-domains: wetness, semi-wetness, aridity, and semi-aridity. The regionalization of these sub-domains followed the results of Ma and Fu (2005), in which extreme aridity is denoted as aridity and extreme wetness as wetness.

Tables 5 and 6 show the annual variations in surface temperature and precipitation in these climate sub-domains. From Tables 5 and 6, the climate effects caused by aerosols in all of these sub-domains were decreases in both temperature and precipitation for all cases.

The decrease magnitude of surface temperature was the largest in the wet region, reaching –0.2 K. The wet region included South and East China and the Sichuan basin, where the aerosols were highly concentrated. The climate effects in this wet region were significant. The semi-wet and semi-arid regions had similar declines in surface temperature, reaching approximately –0.1 K. The arid region had low concentrations of aerosols and exhibited a temperature decrease of merely –0.03 K. The decreases for IM were always larger than those for EM over nearly all of the sub-domains except in arid regions. The temperature variations over China were approximately –0.078, –0.074, and –0.069 K for IM, IEM, and EM, respectively.

Table 5. Annual surface temperature variations in sub-domains

Surface temperature changes (°C)	EM	IM	IEM
Aridity	–0.032	–0.031	–0.032
Semi-aridity	–0.093	–0.116	–0.113
Semi-wetness	–0.087	–0.123	–0.102
Wetness	–0.230	–0.247	–0.221
China	–0.069	–0.078	–0.074

Table 6. Annual precipitation variations in sub-domains

Precipitation changes (mm)	EM	IM	IEM
Aridity	–3.0	–3.6	–2.3
Semi-aridity	–12.8	–21.4	–12.1
Semi-wetness	–50.0	–47.6	–28.5
Wetness	–44.3	–39.2	–98.2
China	–19.0	–20.5	–23.2

The variations in precipitation were more complex than variations in surface temperature. For EM and IM, the most dramatic reductions of precipitation occurred in semi-wet regions. The reductions were about 50.0 and 47.6 mm in semi-wet regions for EM and IM, respectively. The precipitation reductions for EM were larger than for IM in semi-wet and wet regions although the opposite was true in semi-arid and arid regions. As for IEM, the reduction was the largest in wet regions at 98.2 mm. The variations for IEM were less than that for IM or EM in the sub-domains when excluding the wet region.

The seasonal trends of surface temperature changes were similar for the cases of EM, IM, and IEM. The surface temperature reductions were maximal in winter (DJF) and minimal in summer (JJA), consistent with the results of Qian et al. (2003) and Huang et al. (2007). The declines of precipitation were maximal in summer (JJA) and minimal in winter (DJF) for IM and IEM. Huang et al. (2007) also obtained the same variation tendency. The magnitudes of surface temperature and precipitation changes in the study reported by Huang et al. (2007) were larger than those found in this study, and the trend of variations in precipitation for EM was opposite to that for IM and EM.

4. Conclusions and discussion

In this paper, we used RIEMS 2.0 to simulate the distributions of anthropogenic sulfate, BC, and OC and analyzed their impacts on the East Asian climate under external mixing, internal mixing, and partial internal mixing scenarios. Additionally, we analyzed the discrepancies in concentrations of aerosols and the resulting climate effects of aerosols. The main conclusions are summarized as follows:

(1) The mass concentration of sulfate was sensitive to mixing assumptions, with the regional average column burden changing from 6.15 mg m^{-2} when externally mixed to 11.45 mg m^{-2} when internally

mixed. The column burden of sulfate was 10.29 mg m^{-2} for IEM. Sulfate was primarily distributed over East China in all simulations.

(2) Carbonaceous aerosols were much less sensitive to the mixing states. The distributions and average column burdens of carbonaceous aerosols were similar under various mixing scenarios. For the EM case, the column burden of BC and OC were 0.45 and 2.16 mg m^{-2}, respectively. BC and OC were also mainly concentrated over East China, with the higher concentrations occurring in the Sichuan basin and Shanxi Province.

(3) Simulated concentrations of sulfate and carbonaceous aerosols agreed with the observations in magnitude over a variety of measurement sites in East Asia. The discrepancies for sulfate between modeled results and observed results were smaller than those for carbonaceous aerosols. The simulated aerosol concentrations were somewhat closer to the observations for IM than for EM.

(4) The values of radiative forcing at the top of the atmosphere due to anthropogenic aerosols were always negative over the domain for all simulated cases. The RF values were maximal in summer, whereas the values as well as the variations were less in autumn and winter. RF values due to internal mixtures were larger than those of external mixtures in most months, and RF increased from –1.27 W m^{-2} in an external mixing state to –1.97 W m^{-2} in an internal mixing state. The NRF decreased from –0.145 to –0.139 W mg^{-1}.

(5) The climate effects of aerosols were more significant when sulfate and carbonaceous aerosols were internally mixed. The surface air temperature variations over the domain due to the anthropogenic aerosols were –0.067, –0.078, and –0.072 K for external mixing, internal mixing, and partial internal mixing states, respectively. The changes in annual precipitation were –8.0 (EM), –20.6 (IM), and –21.9 mm (IEM) (Table 7). The seasonal trends of surface temperature changes were similar for the three cases, with maximal reductions in winter (DJF) and minimal reductions in summer (JJA). Meanwhile, precipitation declines were minimal in winter (DJF) and maximal in summer (JJA) for IM and IEM. The trend of variations in precipitation for EM was opposite to that for IM and IEM.

Table 7. Seasonal climate effects due to anthropogenic aerosols

	DJF	MAM	JJA	SON	Annual
ΔT (K)					
EM	–0.145	–0.068	–0.013	–0.041	–0.067
IM	–0.146	–0.063	–0.045	–0.060	–0.078
IEM	–0.140	–0.062	–0.039	–0.046	–0.072
ΔP (mm $month^{-1}$)					
EM	–1.449	–0.679	–0.134	–0.411	–0.668
IM	–1.047	–1.792	–2.803	–1.210	–1.713
IEM	–1.082	–1.770	–2.815	–1.626	–1.823

(6) The decrease magnitude of surface temperature was the largest in the wet region due to the large concentration of aerosols there. The most dramatic reductions of precipitation did not occur in the wet region for EM and IM, but rather appeared in the semi-wet region. Many factors contributed to the large uncertainties in the estimates of impacts on climate due to aerosols, including emissions, heterogeneous reactions on existing particles, size spectrum of aerosols, and the mixing assumptions discussed in this paper.

The mixing assumptions of aerosols adopted in this study may not represent the real mixing state in the atmosphere. However, with the comparative analyses, they provide a useful approximation of variations in climate effects due to the mixing state. Some of the more elaborate aerosol mixing production processes, such as heterogeneous reactions, have not been included in models yet. Further studies on these processes and the representation of a more accurate mixing state of aerosols are needed.

REFERENCES

Adhikary, B., S. Kulkarni, A. Dallura, et al., 2008: A regional scale chemical transport modeling of Asian aerosols with data assimilation of AOD observations using optimal interpolation technique. *Atmos. Environ.*, **42**, 8600–8615.

Andreae, M. O., O. Schmid, H. Yang, et al., 2008: Optical properties and chemical composition of the atmospheric aerosol in urban Guangzhou, China. *Atmos.*

Environ., **42**, 6335–6350.

Bergin, M. H., G. R. Cass, J. Xu, et al., 2001: Aerosol radiative, physical, and chemical properties in Beijing during June 1999. *J. Geophys. Res.*, **106**, 17969–17980.

Bohren, C. F., and D. R. Hoffman, 1983: *Absorption and Scattering of Light by Small Particles.* John Wiley & Sons, Inc., 287–324.

Cao, J. J., Z. X. Shen, J. C. Chow, et al., 2009: Seasonal variations and sources of mass and chemical composition for PM10 aerosol in Hangzhou, China. *Particuology*, **7**(3), 161–168.

Chang, L. S., and S. U. Park, 2004: Direct radiative forcing due to anthropogenic aerosols in East Asia during April 2001. *Atmos. Environ.*, **38**, 4467–4482.

Chang, S. C., C. C. K. Chou, C. C. Chan, et al., 2010: Temporal characteristics from continuous measurements of PM2.5 and speciation at the Taipei Aerosol Supersite from 2002 to 2008. *Atmos. Environ.*, **44**, 1088–1096.

Chung, S. H., and J. H. Seinfeld, 2005: Climate response of direct radiative forcing of anthropogenic black carbon. *J. Geophys. Res.*, **110**, D11102, doi:10.1029/2004JD005441.

Chung, C. E., V. Ramanathan, D. Kim, et al., 2005: Global anthropogenic aerosol direct forcing derived from satellite and ground-based observations. *J. Geophys. Res.*, **110**, D24207, doi: 10.1029/2005JD006356.

——, V. Ramanathan, G. Carmichael, et al., 2010: Anthropogenic aerosol radiative forcing in Asia derived from regional models with atmospheric and aerosol data assimilation. *Atmos. Chem. Phys.*, **10**, 6007–6024.

Ebert, M., S. Weinbruch, A. Rausch, et al., 2002: The complex refractive index of aerosols during LACE 98 as derived from the analysis of individual particles. *J. Geophys. Res.*, **107**, 8121, doi:10.1029/2000JD000195.

Fassi-Fihri, A., K. Suhre, and R. Rosset, 1997: Internal and external mixing in atmospheric aerosols by coagulation: impact on the optical and hygroscopic properties of the sulfate-soot system. *Atmos. Environ.*, **31**, 1393–1402.

Fu, C. B., H. L. Wei, and Y. Qian, 2000: Documentation on regional integrated environmental model system (RIEMS). TEACOM Science Report, No. 122.

——, S. Y. Wang, Z. Xiong, et al., 2005: Regional climate model inter comparison project for Asia. *Bull. Amer. Meteor. Soc.*, **86**(2), 257–266.

Gelbard, F., Y. Tambour, and J. H. Seinfeld, 1980: Sectional representations for simulating aerosol dynamics. *J. Colloid Interface Sci.*, **76**(2), 541–556.

Ghan, S. J., R. C. Easter, E. G. Chapman, et al., 2001: A physically based estimate of radiative forcing by anthropogenic sulfate aerosol. *J. Geophys. Res.*, **106**(D6), doi:10.1029/2000JD900503.

Giorgi, F., X. Q. Bi, and Y. Qian, 2002: Direct radiative forcing and regional climatic effects of anthropogenic aerosols over East Asia: A regional coupled climate-chemistry/aerosol model study. *J. Geophys. Res.*, **107**(D20), 4439, doi:10.1029/2001JD001066.

——, ——, and ——, 2003: Indirect vs. direct effects of anthropogenic sulfate on the climate of East Asia as simulated with a regional coupled climate-chemistry/aerosol model. *Climatic Change*, **58**, 345–376.

Gu, Y., K. N. Liou, Y. Xue, et al., 2006: Climatic effects of different aerosol types in China simulated by the UCLA general circulation model. *J. Geophys. Res.*, **111**, 15201, doi: 10.1029/2005JD006312.

Han, Y. M., Z. W. Han, J. J. Cao, et al., 2008: Distribution and origin of carbonaceous aerosol over a rural high-mountain lake area, northern China and its transport significance. *Atmos. Environ.*, **42**, 2405–2414.

Hansen, J., M. Sato, L. Nazarenko, et al., 2002: Climate forcings in Goddard Institute for Space Studies SI2000 simulations. *J. Geophys. Res.*, **107**(D18), 4347, doi: 10.1029/2001JD001143.

Haywood, J. M., and K. P. Shine, 1995: The effect of anthropogenic sulfate and soot aerosol on the clear sky planetary radiation budget. *Geophys. Res. Lett.*, **22**, 603–606.

He, K. B., F. M. Yang, Y. L. Ma, et al., 2001: The characteristics of PM2.5 in Beijing, China. *Atmos. Environ.*, **35**, 4959–4970.

Hegg, D. A., 1994: Cloud condensation nucleus-sulfate mass relationship and cloud albedo. *J. Geophys. Res.*, **99**(D12), 25903–25907.

Heo, J. B., P. K. Hopke, and S. M. Yi, 2009: Source apportionment of PM2.5 in Seoul, Korea. *Atmos. Chem. Phys.*, **9**, 4957–4971.

Han, Z. W., R. J. Zhang, Q. G. Wang, et al., 2008: Regional modeling of organic aerosols over China in summertime. *J. Geophys. Res.*, **113**, 11202, doi:10.1029/ 2007JD009436.

Huang, Y., W. L. Chameides, and R. E. Dickson, 2007: Direct and indirect effects of anthropogenic aerosols on regional precipitation over East Asia. *J. Geophys. Res.*, **112**, 03212, doi:10.1029/2006JD007114.

Intergovernmental Panel on Climate Change (IPCC), 2007: *Fourth Assessment Report of the Intergovernmental Panel on Climate Change*. Cambridge University Press, 153–179.

Jacobson, M. Z., 2001a: Strong radiative heating due to mixing state of black carbon in atmospheric aerosols. *Nature*, **409**, 695–697.

——, 2001b: Global direct radiative forcing due to multicomponent anthropogenic and natural aerosols. *J. Geophys. Res.*, **106**(D2), 1551–1568.

Joseph, C. L., 1993: "BHCOAT", http://atol.ucsd.edu/ ∼pflatau/scatlib/scatlib.htm.

Kiehl, J. T., T. L. Schneider, P. J. Rasch, et al., 2000: Radiative forcing due to sulfate aerosols from simulations with the National Center for Atmospheric Research Community Climate Model, Version 3. *J. Geophys. Res.*, **105**(D1), 1441–1457.

Kim, D., C. Wang, A. M. L. Ekman, et al., 2008: Distribution and direct radiative forcing of carbonaceous and sulfate aerosols in an interactive size-resolving aerosol-climate model. *J. Geophys. Res.*, **113**, 16309, doi:10.1029/ 2007JD009756.

Kim, Y. J., J. H. Wu, Y. I. Ma, et al., 2009: Chemical characteristics of long-range transport aerosol at background sites in Korea. *Atmos. Environ.*, **43**, 5556–5566.

Kim, Y. P., and J. H. Seinfeld, 1990: Simulation of multicomponent aerosol condensation by the moving sectional method. *J. Colloid Interface Sci.*, **135**(1), 185–199.

Kirkevag, A., and T. Iversen, 2002: Global direct radiative forcing by process-parameterized aerosol optical properties. *J. Geophys. Res.*, **107**(D20), 4433, doi:10.1029/2001JD000886.

Lesins, G., P. Chylek, and U. Lohmann, 2002: A study of internal and external mixing scenarios and its effect on aerosol optical properties and direct radiative forcing. *J. Geophys. Res.*, **107**(D10), 4094, doi:10.1029/2001JD000973.

Li, W. J., L. Y. Shao, Z. S. Wang, et al., 2010: Size, composition, and mixing state of individual aerosol particles in a South China coastal city. *J. Environ. Sci.*, **22**(4), 561–569.

Liao, H., and J. H. Seinfeld, 2005: Global impacts of gas-phase chemistryaerosol interactions on direct radiative forcing by anthropogenic aerosols and ozone. *J. Geophys. Res.*, **110**(D18), 18208, doi: 10.1029/2005JD005907.

Liu, H. N., L. Zhang, and J. Wu, 2010: A modeling study of climate effect of sulfate and carbonaceous aerosols over China. *Adv. Atmos. Sci.*, **27**(6), 1276–1288.

Liu, X., J. E. Penner, B. Das, et al., 2007: Uncertainties in global aerosol simulations: Assessment using three meteorological data sets. *J. Geophys. Res.*, **112**, 11212, doi: 10.1029/2006JD008216.

Lu, J., and F. M. Bowman, 2010: A detailed aerosol mixing state model for investigating interactions between mixing state, semivolatile partitioning, and coagulation. *Atmos. Chem. Phys.*, **10**, 4033–4046.

Ma, Z. G., and C. B. Fu, 2005: Decade variations of arid and semi-arid boundary in China. *Chinese J. Geophys.*, **48**(3), 519–525. (in Chinese)

Manktelow, P. T., G. W. Mann, K. S. Carslaw, et al., 2007: Regional and global trends in sulfate aerosol since the 1980s. *Geophys. Res. Lett.*, **34**, L14803, doi:10.1029/2006GL028668.

Meng, Z. Y., X. M. Jiang, P. Yan, et al., 2007: Characteristics and sources of PM2.5 and carbonaceous species during winter in Taiyuan, China. *Atmos. Environ.*, **41**, 6901–6908.

Moteki, N., and Y. Kondo, 2007a: Effects of mixing state on black carbon measurement by laser-induced incandescence. *Aerosol Sci. Technol.*, **41**, 398–417, doi 10.1080/02786820701199728.

——, ——, Y. Miyazaki, et al., 2007b: Evolution of mixing state of black carbon particles: Aircraft measurements over the western Pacific in March 2004. *Geophys. Res. Lett.*, **34**, L11803, doi: 10.1029/2006GL028943.

Naoe, H., and K. Okada, 2001: Mixing properties of submicrometer aerosol particles in the urban atmosphere-with regard to soot particles. *Atmos. Environ.*, **35**, 5765–5772.

Novakov, T., S. Menon, T. W. Kirchstetter, et al., 2005: Aerosol organic carbon to black carbon ratios: Analysis of published data and implications

for climate forcing. *J. Geophys. Res.*, **110**, 21205, doi:10.1029/2005JD005977.

Okuda, T., S. Nakao, M. Katsuno, et al., 2008: Trends in hazardous trace metal concentrations in aerosols collected in Beijing, China from 2001 to 2006. *Chemosphere*, **72**, 917–924.

Pathak, R. K., W. S. Wu, and T. Wang, 2009: Summertime PM2.5 ionic species in four major cities of China: Nitrate formation in an ammonia-deficient atmosphere. *Atmos. Chem. Phys.*, **9**, 1711–1722.

Penner, J. E., R. Dickinson, and C. O'Neill, 1992: Effects of aerosol from biomass burning on the global radiation budget. *Science*, **256**, 1432–1432.

——, C. C. Chuang, and K. Grant, 1998: Climate forcing by carbonaceous and sulfate aerosol. *Climate Dyn.*, **14**, 839–851.

Qian, Y., F. Giorgi, Y. Huang, et al., 2001: Regional simulation of anthropogenic sulfur over East Asia and its sensitivity to model parameters. *Tellus*, **53B**, 171–191.

——, L. R. Leung, S. J. Ghan, et al., 2003: Regional climate effects of aerosols over China: Modeling and observation. *Tellus*, **55B**, 914–934.

Qu, W. J., X. Y. Zhang, R. Arimoto, et al., 2009: Aerosol background at two remote CAWNET sites in western China. *Science of the Total Environment*, **407**, 3518–3529.

Reddy, M. S., and O. Boucher, 2004: A study of the global cycle of carbonaceous aerosols in the LMDZT general circulation model. *J. Geophys. Res.*, **109**(D14), 14202, doi: 10.1029/2003JD004048.

Schulz, M., C. Textor, S. Kinne, et al., 2006: Radiative forcing by aerosols as derived from the AeroCom present-day and pre-industrial simulations. *Atmos. Chem. Phys.*, **6**, 5225–5246.

Schwarz, J. P., J. R. Spackman, D. W. Fahey, et al., 2008: Coatings and their enhancement of black carbon light absorption in the tropical atmosphere. *J. Geophys. Res.*, **113**, 03203, doi:10.1029/2007JD009042.

Shiraiwa, M., Y. Kondo, N. Moteki, et al., 2007: Evolution of mixing state of black carbon in polluted air from Tokyo. *Geophys. Res. Lett.*, **34**, L16803, doi:10.1029/2007GL029819.

——, ——, ——, et al., 2008: Radiative impact of mixing state of black carbon aerosol in Asian outflow. *J. Geophys. Res.*, **113**, 24210, doi: 10.1029/2008JD010546.

So, K, L., H. Guo, and Y. S. Li, 2007: Long-term variation of PM2.5 levels and composition at rural, urban, and roadside sites in Hong Kong: Increasing impact of regional air pollution. *Atmos. Environ.*, **41**, 9427–9434.

Stier, P., J. Feichter, S. Kinne, et al., 2005: The aerosol-climate model ECHAM5-HAM. *Atmos. Chem. Phys.*, **5**, 1125–1156.

——, H. Seinfeld, S. Kinne, et al., 2006: Impact of nonabsorbing anthropogenic aerosols on clear-sky atmosphere absorption. *J. Geophys. Res.*, **111**, 18201, doi:10.1029/ 2006JD007147.

Streets, D. G., C. Yu, Y. Wu, et al., 2008: Aerosol trends over China, 1980–2000. *Atmos. Res.*, **88**, 174–182.

Strom, J., K. Okada, and J. Heintzenberg, 1992: On the state of mixing of particles due to brownian coagulation. *J. Aerosol Sci.*, **23**, I5, 467–480.

Tan, Q., W. L. Chameides, D. Streets, et al., 2004: An evaluation of TRACE-P emission inventories from China using a regional model and chemical measurements. *J. Geophys. Res.*, **109**, 22305, doi: 10.1029/2004JD005071.

Vester, B. P., M. Ebert, E. B. Barnert, et al., 2007: Composition and mixing state of the urban background aerosol in the Rhein-Main Area (Germany). *Atmos. Environ.*, **41**, 6102–6115.

Warren, D. R., and J. H. Seinfeld, 1985: Simulation of aerosol size distribution evolution in systems with simultaneous nucleation, condensation and coagulation. *Aerosol Sci. Technol.*, **4**, 31–43.

Worringen, A., M. Ebert, T. Trautmann, et al., 2008: Optical properties of internally mixed ammonium sulfate and soot particles: A study of individual aerosol particles and ambient aerosol populations. *Appl. Optics.*, **47**(21), 3835–3845.

Wu, J., Y. Luo, and W. G. Wang, 2005: The comparison of different simulation methods for the radiative forcing of anthropogenic sulfate aerosol over East Asia. *Journal of Yunnan University (Natural Sciences)*, **27**(4), 323–331. (in Chinese)

Xie, S. D., Z. Liu, T. Chen, and L. Hua, 2008: Spatiotemporal variations of ambient PM10 source contributions in Beijing in 2004 using positive matrix factorization. *Atmos. Chem. Phys.*, **8**, 2701–2716.

Xiong, Z., 2004: The multiyear surface climatology of RIEMS over East Asia. *Climatic Environ. Res.*, **9**(2), 251–260. (in Chinese)

——, S. Y. Wang, Z. M. Zeng, et al., 2003: Analysis of simulation heavy rain over the Yangtze River valley during 11–30 June 1998 using RIEMS. *Adv. Atmos. Sci.*, **20**, 815–824.

——, C. B. Fu, and Q. Zhang, 2006: On the ability of the regional climate model RIEMS to simulate the present climate over East Asia. *Adv. Atmos. Sci.*, **23**(5), 784–791.

——, C. B. Fu, and X. D. Yan, 2009: Regional integrated environmental model system and its simulation of East Asian summer monsoon. *Chinese Sci. Bull.*, **54**, 4253–4261.

Xu, J., M. H. Bergin, X. Yu, et al., 2002: Measurement of aerosol chemical, physical and radiative properties in the Yangtze Delta region of China. *Atmos. Environ.*, **36**, 161–173.

Ye, B., X. L. Ji, H. Z. Yang, et al., 2003: Concentration and chemical composition of PM2.5 in Shanghai for a 1-year period. *Atmos. Environ.*, **37**, 499–510.

Yu, H., Y. J. Kaufman, M. Chin, et al., 2006: A review of measurement-based assessments of aerosol direct radiative effect and forcing. *Atmos. Chem. Phys.*, **6**, 613–666.

Yu, J. Z., J. W. T. Tung, A. W. M. Wu, et al., 2004: Abundance and seasonal characteristics of elemental and organic carbon in Hong Kong PM10. *Atmos. Environ.*, **38**, 1511–1521.

Zhang, H., Z. L. Wang, P. W. Guo, et al., 2009a: A modeling study of the effects of direct radiative forcing due to carbonaceous aerosol on the climate in East Asia. *Adv. Atmos. Sci.*, **26**(1), 57–66.

Zhang, Q., D. G. Streets, et al., 2009b: Asian emissions in 2006 for the NASA INTEX-B mission. *Atmos. Chem. Phys.*, **9**, 5131–5153.

Zhang, X. Y., Y. Q. Wang, X. C. Zhang, et al., 2008: Carbonaceous aerosol composition over various regions of China during 2006. *J. Geophys. Res.*, **113**, 14111, doi:10.1029/2007JD009525.

Zhou, M., H. Yu, R. E. Dickinson, et al., 2005: A normalized description of the direct effect of key aerosol types on solar radiation as estimiated from AERONET. *J. Geophys. Res.*, **110**, 19202, doi:10.1029/2005JD005909.